Adsorption of Diclofenac onto MOF-Based Adsorbents: Kinetic, Equilibrium, and Thermodynamic Insights in a Controlled Non-Aqueous Medium

Santiago N. Bulla-Martínez[1,2], Marisol Ramos[2], Liliana Giraldo[3], Juan Carlos Moreno-Piraján[1],*

[1] Departamento de Química, Grupo de Investigación en Sólidos Porosos y Calorimetría,

Universidad de los Andes, Bogotá, Colombia

[2] Departamento de Química, Universidad Distrital "Francisco José de Caldas", Bogotá, Colombia

[3] Departamento de Química, Grupo de Calorimetría, Universidad Nacional de Colombia, Sede Bogotá, Colombia

* Corresponding author: *jumoreno@uniandes.edu.co*

Abstract

Pharmaceutical micropollutants, including non-steroidal anti-inflammatory drugs such as diclofenac, persist in aquatic environments after conventional wastewater treatment, posing chronic ecological and public health risks. Metal–organic frameworks (MOFs) are among the most promising adsorbent platforms for their removal; however, a pervasive methodological limitation in the published literature undermines the reliability of reported adsorption parameters. The hydrolytic instability of archetypal frameworks such as HKUST-1 ($Cu_3(BTC)_2$) and MOF-5 ($Zn_4O(BDC)_3$) in aqueous media leads to concurrent structural degradation that is systematically conflated with adsorption, rendering thermodynamic and kinetic data mechanistically ambiguous. To resolve this issue, the present work employs a strictly controlled non-aqueous medium (absolute ethanol), in which both frameworks retain their crystalline integrity, thereby isolating intrinsic adsorbate–framework interactions.

Both materials were synthesized by reflux and comprehensively characterized by PXRD, FTIR, Raman spectroscopy, SEM, and N_2 physisorption at 77 K. Their hydrolytic sensitivity was systematically evaluated across pH 3–9 before all adsorption experiments, providing unambiguous experimental justification for the non-aqueous experimental design. Among the three isotherm models evaluated, the Sips equation provided the best statistical fit ($R^2 > 0.97$ for both materials), consistent with energetically heterogeneous surfaces. MOF-5 achieved a higher maximum adsorption capacity (195.28 mg g^{-1}), attributable to its larger surface area (2886 m^2 g^{-1}) and pore volume; HKUST-1 exhibited stronger initial adsorption affinity driven by coordinatively unsaturated Cu(II) open metal sites. Pseudo-first-order kinetics and multilinear Weber–Morris plots indicated a multistep transport mechanism in which external mass transfer and intraparticle diffusion act as co-limiting steps. Thermodynamic analysis confirmed spontaneous and exothermic adsorption for both materials: HKUST-1 displayed chemisorption characteristics ($\Delta H° = -48.6$ kJ mol^{-1}), while MOF-5 fell within the physisorption regime ($\Delta H° = -21.4$ kJ mol^{-1}). The non-aqueous strategy provides a reproducible and transparent platform for establishing structure–property relationships essential to the rational design of water-stable MOF variants for sustainable wastewater treatment.

Keywords: diclofenac adsorption; metal–organic frameworks; non-aqueous medium; HKUST-1; MOF-5; pharmaceutical micropollutants; adsorption thermodynamics; sustainable wastewater treatment; cleaner waste systems

1. Introduction

The discharge of pharmaceutical residues into aquatic environments is a growing global environmental concern. Unlike classical priority pollutants, active pharmaceutical ingredients — including analgesics, antibiotics, and hormones — enter water bodies through multiple, essentially continuous pathways: incomplete metabolic elimination, disposal of unused medications, and the inherent removal limitations of conventional municipal wastewater treatment plants (Kümmerer, 2009; Barbosa et al., 2016). Once in receiving waters, these compounds persist at concentrations that, although sub-therapeutic, are sufficient to disrupt endocrine function, promote antibiotic resistance, and cause chronic ecotoxicological effects on non-target aquatic organisms (Verlicchi et al., 2012). Among pharmaceuticals detected in treated effluents and surface waters worldwide, diclofenac — a widely prescribed non-steroidal anti-inflammatory drug — has attracted particular regulatory attention and was listed as a priority substance under the European Water Framework Directive because of its high consumption volume, chemical stability, and resistance to biological degradation (European Commission, 2013; Ternes, 1998). Its routine detection in drinking water precursors underscores the fundamental inadequacy of existing treatment infrastructure in addressing chemically diverse emerging contaminants (Hernando et al., 2006).

Adsorption onto high-surface-area porous materials is widely recognized as one of the most effective, operationally flexible, and scalable strategies for removing trace organic contaminants from water (Ali, 2012). Among the adsorbent candidates explored over the past decade, metal–organic frameworks (MOFs) — crystalline, three-dimensional coordination networks formed through the self-assembly of metal nodes or clusters with polyfunctional organic linkers — have attracted exceptional interest (Furukawa et al., 2013; Li et al., 1999). Their record-high specific surface areas, engineerable pore geometries, and the possibility of incorporating chemically active binding sites directly within the framework architecture make them, in principle, ideal materials for selectively concentrating pharmaceutical molecules from dilute aqueous streams (Zhao et al., 2018). A growing body of work has demonstrated the capacity of MOFs to remove diclofenac and structurally related pharmaceuticals (Prasetya and Li, 2021; Zhuang et al., 2019; Cresпí Sánchez et al., 2023). However, most of these evaluations are conducted in aqueous systems without rigorously verifying the structural stability of the adsorbent under the prevailing experimental conditions, thereby introducing a systematic, largely unacknowledged source of uncertainty that profoundly compromises the reliability and comparability of reported adsorption parameters (DeCoste et al., 2012).

This problem is particularly acute for archetypal, moisture-sensitive frameworks such as HKUST-1 (also designated MOF-199, $Cu_3(BTC)_2$, where BTC = 1,3,5-benzenetricarboxylate) and MOF-5 ($Zn_4O(BDC)_3$, IRMOF-1, where BDC = 1,4-benzenedicarboxylate). Both materials are among the most widely cited in the adsorption literature for their well-defined pore architectures and exceptionally high accessible surface areas. Yet both exhibit well-documented hydrolytic sensitivity: HKUST-1 undergoes progressive pore collapse and partial Cu leaching under humid or aqueous conditions (Kúsgens et al., 2009; Schoenecker et al., 2012), while MOF-5 amorphizes rapidly above pH 5 through attack on the Zn–carboxylate coordination bonds (Huang et al., 2003; Greathouse and Allendorf, 2006). When adsorption experiments are performed on such materials in aqueous systems without pre-verification of structural integrity, the measured uptake inevitably reflects a superposition of genuine adsorption and material transformation. This renders thermodynamic and kinetic parameters ambiguous and potentially misleading for rational material design — a gap this work is designed to address. Controlled non-aqueous media offer a relevant yet underexplored pathway to resolving this ambiguity. By replacing water with a solvent in which the target adsorbate is freely soluble but the MOF framework remains structurally intact, it becomes possible to measure equilibrium, kinetics, and thermodynamics under conditions that genuinely reflect the material's intrinsic properties. Absolute ethanol satisfies these dual requirements for both HKUST-1 and MOF-5: diclofenac dissolves readily across the concentration range of interest, and both frameworks retain their crystalline structure and porosity throughout the experimental campaign, as confirmed by post-adsorption PXRD and FTIR. This approach does not supplant aqueous studies — which remain the practically relevant context for wastewater treatment — but provides a consistent reference framework for understanding structure–property relationships and for guiding the rational design of more water-stable MOF derivatives (Wang et al., 2015; Canivet et al., 2014). Prior to adsorption experiments, the hydrolytic behavior of HKUST-1 and MOF-5 was systematically characterized across pH 3–9 using post-immersion PXRD, FTIR, and BET analysis, establishing the experimental justification for this design choice.

From the perspective of sustainable waste management — central to this journal's scope — developing reliable removal strategies for pharmaceutical micropollutants requires not only improving material performance but also deepening mechanistic understanding to enable predictive design. The present work is situated at this intersection: adsorption equilibrium was modeled using Langmuir (Langmuir, 1918), Freundlich (Freundlich, 1906), and Sips (Sips, 1948) isotherms; kinetics were analyzed with pseudo-first-order (Lagergren, 1898), pseudo-second-order (Ho and McKay, 1999), and Elovich (Elovich and Larionov, 1962) models, complemented by Weber–Morris intraparticle diffusion analysis (Weber and Morris, 1963); and thermodynamic parameters were extracted from van't Hoff plots at four temperatures (Liu, 2009). The resulting self-consistent dataset enables a rigorous, comparative assessment of the two frameworks and provides a basis for advancing MOF-based pharmaceutical removal as part of cleaner, more sustainable wastewater treatment strategies.

2. Materials and Methods

2.1 Reagents

Diclofenac sodium (≥99% purity) was used as received, without further purification. Copper(II) acetate monohydrate and zinc nitrate hexahydrate served as metal precursors for HKUST-1 and MOF-5, respectively. 1,3,5-Benzenetricarboxylic acid (H_3BTC, trimesic acid) and 1,4-benzenedicarboxylic acid (H_2BDC, terephthalic acid) were analytical grade. N,N-Dimethylformamide (DMF) and ethanol (analytical grade) were used as synthesis and washing solvents. All adsorption experiments were conducted exclusively in absolute ethanol (analytical grade, water content < 0.01% v/v) to maintain rigorously anhydrous conditions throughout.

2.2 Synthesis of HKUST-1 and MOF-5

Both materials were synthesized by a reflux-based method adapted from established solvothermal procedures (Chui et al., 1999; Li et al., 1999) and refined to improve crystallinity and batch-to-batch reproducibility without requiring autoclave equipment. HKUST-1 was prepared by dissolving copper(II) acetate monohydrate and H_3BTC in a mixed ethanol/DMF/water solvent system under continuous magnetic stirring; the solution was refluxed at a controlled temperature for 12 h. The blue-green crystalline product was collected by vacuum filtration, washed exhaustively with fresh DMF and ethanol to remove unreacted reagents and occluded linker molecules, and then dried at 80 °C under vacuum. MOF-5 was synthesized from zinc nitrate hexahydrate and H_2BDC in DMF and refluxed for 24 h; the white microcrystalline solid was collected by filtration, washed with DMF and chloroform to remove unreacted species, and dried under analogous conditions. Prior to all characterization and adsorption experiments, both materials were thermally activated under dynamic vacuum ($< 10^{-2}$ mbar) — at 150 °C for HKUST-1 and 200 °C for MOF-5 — for at least 12 h to fully evacuate guest solvent molecules from the pore network and ensure maximum framework accessibility (Yaghi et al., 2003).

2.3 Characterization and Hydrolytic Stability Assessment

Crystalline phase purity was confirmed by powder X-ray diffraction (PXRD) using Cu Kα radiation (λ = 1.5406 Å) over 2θ = 5–40°. Fourier-transform infrared (FTIR) spectra were recorded in attenuated total reflectance (ATR) mode over 400–4000 cm^{-1} to identify metal–ligand coordination bands. Raman spectra were acquired with a 532 nm laser to characterize lattice dynamics and secondary building unit (SBU) connectivity. Morphology and particle-size distributions were examined by scanning electron microscopy (SEM) at 10 kV after sputter-coating with gold. Textural parameters — BET surface area (Brunauer et al., 1938), micropore volume (t-plot), total pore volume (P/P_0 = 0.99), and DFT pore-size distributions — were derived from N_2 adsorption–desorption isotherms at 77 K after degassing at the respective activation temperatures (Lowell et al., 2004). Hydrolytic stability was assessed by suspending each material in aqueous phosphate-buffered solutions at pH 3, 5, 7, and 9 (without added diclofenac) and stirring for 24 h at 25 °C. Recovered solids were then dried at 80 °C and re-characterized by PXRD, FTIR, and N_2 physisorption. Structural integrity was evaluated against three independent criteria: (i) preservation of characteristic diffraction peak positions and relative intensities; (ii) retention of key metal–ligand FTIR bands; and (iii) maintenance of BET surface area within 10% of the as-synthesized value (Schoenecker et al., 2012). These data establish the operational pH window for each material and provide the primary justification for the non-aqueous adsorption protocol.

2.4 Preparation of Solutions and Anhydrous Experimental Conditions

Stock solutions of diclofenac sodium in absolute ethanol were prepared at concentrations up to 500 mg L^{-1} and diluted immediately before each experiment. All glassware was oven-dried at 120 °C and stored over activated molecular sieves. Absolute ethanol was transferred and stored in sealed containers under a dry nitrogen atmosphere. Adsorption experiments were conducted in stoppered Erlenmeyer flasks to minimize exposure to ambient humidity. The residual water content of the solvent was periodically measured by Karl Fischer coulometric titration; all values remained below 0.02% (v/v) throughout the experimental campaign, confirming that the observed adsorption behavior reflected intrinsic adsorbate–framework interactions rather than hydrolytically induced structural changes (Canivet et al., 2014).

2.5 Batch Adsorption Experiments and Equilibrium Isotherms

Batch adsorption experiments were conducted by contacting a fixed mass of activated adsorbent (m = 10 mg) with 25 mL of diclofenac solution in absolute ethanol at controlled temperature and 180 rpm orbital agitation. Equilibrium isotherms were constructed at 298 K by varying the initial concentration from 10 to 500 mg L^{-1}, with a contact time of 720 min, which was confirmed adequate by preliminary kinetic experiments. Suspensions were separated by centrifugation (3000 rpm, 10 min) and, when necessary, filtered through 0.45 µm PTFE membranes before spectrophotometric analysis. Residual diclofenac concentrations were quantified by UV–Vis spectroscopy at λmax = 276 nm; calibration curves over the working concentration range yielded $R^2 > 0.999$. The equilibrium adsorption capacity qe (mg g^{-1}) was calculated from the mass balance:

$$q_e = \frac{(C_o - C_e).V}{m}$$

where C_0 and Ce are the initial and equilibrium diclofenac concentrations (mg L^{-1}), V is the solution volume (L), and m is the adsorbent mass (g). Experimental data were fitted to the Langmuir (Langmuir, 1918), Freundlich (Freundlich, 1906), and Sips (Sips, 1948) isotherm models using nonlinear least-squares regression; model discrimination was based on R^2, root mean square error (RMSE), and the Akaike information criterion (AIC).

2.6 Adsorption Kinetics

Kinetic experiments were conducted at an initial diclofenac concentration of 100–150 mg L^{-1} and at 298 K. Aliquots were collected at predetermined intervals from 0 to 720 min, immediately centrifuged, and analyzed spectrophotometrically. The amount adsorbed at time t (qt, mg g^{-1}) was calculated by mass balance. Data were analyzed using the pseudo-first-order (Lagergren, 1898), pseudo-second-order (Ho and McKay, 1999), and Elovich (Elovich and Larionov, 1962) models via nonlinear regression. The intraparticle diffusion mechanism was elucidated using the Weber–Morris model (Weber and Morris, 1963), which plots qt against $t^{0.5}$. Multilinear profiles were interpreted as successive stages of external film diffusion (Zone I), intraparticle diffusion (Zone II), and equilibrium (Zone III).

2.7 UV–Vis Quantification of Diclofenac

Diclofenac concentrations were determined by UV–Vis spectrophotometry. A full spectral scan (200–400 nm) in absolute ethanol identified the absorption maximum at λmax = 276 nm. Calibration curves across the working concentration range showed excellent linearity ($R^2 > 0.999$). Solvent blanks were used for baseline correction. Only clear, particle-free supernatants — filtered through 0.45 µm PTFE membranes when necessary — were analyzed to eliminate light-scattering artifacts.

2.8 Thermodynamic Analysis

Thermodynamic parameters were derived from adsorption data collected at 283, 288, 293, and 298 K. The dimensionless equilibrium constant Kc was computed from the Sips isotherm parameters at each temperature. The standard Gibbs free energy change was calculated using $\Delta G^\circ = -RT \ln Kc$, while the standard enthalpy (ΔH°) and entropy (ΔS°) changes were obtained from the slope and intercept, respectively, of the linear van't Hoff plot of ln Kc versus 1/T (Liu, 2009). Kc was expressed in strictly dimensionless form to ensure thermodynamic consistency of the computed parameters.

3. Results and Discussion

3.1 Structural and Chemical Validation of HKUST-1 and MOF-5

Crystalline integrity was first confirmed by PXRD. The diffraction pattern of HKUST-1 (Fig. 1) shows well-defined low-angle reflections consistent with the face-centered cubic Cu–BTC framework (space group $Fm\bar{3}m$), in full agreement with the structure originally reported by Chui et al. (1999). The dominant reflections, indexed as (200), (220), (222), and (400), align closely with the reference pattern shown in the inset, confirming the formation of paddle-wheel $Cu_2(COO)_4$ secondary building units and long-range structural periodicity. No additional peaks associated with secondary phases or copper oxides were detected, establishing high phase purity. The PXRD pattern of MOF-5 (Fig. 2) exhibits sharp, symmetric reflections indexed as (200), (220), (222), and (400), in accordance with the cubic MOF-5 topology first reported by Li et al. (1999). The excellent correspondence with the literature reference further validates the reflux-based synthesis route as a reliable, autoclave-free approach yielding structurally robust MOFs suitable for adsorption studies (Yaghi et al., 2003).

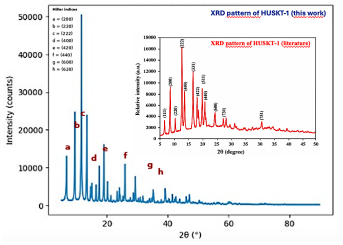

Fig. 1. PXRD pattern of HKUST-1 synthesized in this work, with indexed reflections consistent with the cubic Cu–BTC framework (space group $Fm\bar{3}m$). Inset: reference diffraction pattern from Chui et al. (1999) for comparison.

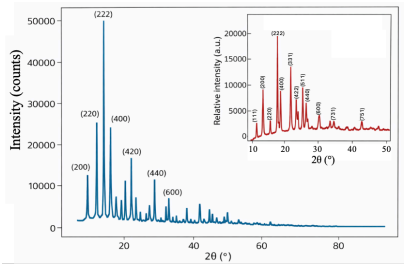

Fig. 2. PXRD pattern of MOF-5 synthesized under reflux conditions, with indexed reflections confirming formation of the characteristic cubic crystalline framework. Inset: reference diffraction pattern from Li et al. (1999) for comparison.

3.2 Vibrational Analysis and Coordination Environment

FTIR spectra (Figs. 3 and 4) provide complementary evidence for framework formation and effective metal–linker coordination. For HKUST-1 (Fig. 3), intense bands at approximately 1643–1550 cm^{-1} are assigned to the asymmetric stretch of coordinated carboxylate groups ($\nu asCOO^-$), and a band near 1446 cm^{-1} corresponds to the symmetric stretch ($\nu sCOO^-$). The absence of a carbonyl absorption near 1700 cm^{-1} — characteristic of protonated carboxylic acid — confirms full deprotonation of H_3BTC and its successful incorporation into the paddle-wheel $Cu_2(COO)_4$ SBUs, consistent with published reference spectra (Chui et al., 1999). For MOF-5 (Fig. 4), characteristic absorptions at approximately 1573 cm^{-1} ($\nu asCOO^-$) and 1369 cm^{-1} ($\nu sCOO^-$) confirm coordination of terephthalate linkers to Zn_4O cluster SBUs (Li et al., 1999). Absorptions in the 800–500 cm^{-1} region are attributed to Zn–O framework stretching modes. Raman spectra (Figs. 5 and 6) provide further insight into lattice dynamics and SBU integrity, consistent with previously reported assignments for both frameworks (Prestipino et al., 2006; Bordiga et al., 2004).

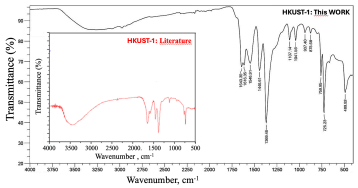

Fig. 3. ATR-FTIR spectrum of HKUST-1 synthesized in this work, showing the absence of a free carbonyl band near 1700 cm^{-1}, indicative of complete deprotonation of the H_3BTC linker. Inset: reference FTIR spectrum from the literature for comparison.

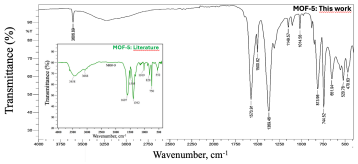

Fig. 4. ATR-FTIR spectrum of MOF-5, showing characteristic carboxylate coordination bands consistent with the $Zn_4O(BDC)_3$ framework. Inset: reference FTIR spectrum from the literature for comparison.

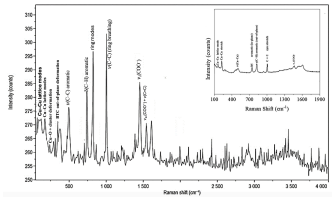

Fig. 5. Raman spectrum of HKUST-1, highlighting lattice vibrations and carboxylate coordination modes associated with the paddle-wheel $Cu_2(COO)_4$ secondary building unit. Inset: reference Raman spectrum from the literature for comparison.

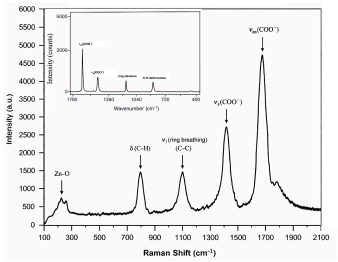

Fig. 6. Raman spectrum of MOF-5, showing characteristic Zn–O vibrations and aromatic ring-breathing modes of the BDC linker. Inset: reference Raman spectrum from the literature for comparison.

3.3 Morphological Features

SEM micrographs (Fig. 7) reveal distinct morphologies that directly reflect the coordination chemistry and crystallization kinetics of each framework. HKUST-1 (Fig. 7a) forms well-defined polyhedral crystals with the characteristic octahedral habit of the Cu–BTC system; particle-size analysis of representative micrographs yields a mean equivalent diameter of approximately 26.7 μm. The uniform size distribution, absence of amorphous debris, and well-resolved crystal faces collectively indicate controlled nucleation and ordered growth — features relevant to batch-to-batch reproducibility and future scale-up. MOF-5 (Fig. 7b) crystallizes as discrete cubic particles with sharp edges and smooth faces, consistent with the high-symmetry $Zn_4O(BDC)_3$ framework (Li et al., 1999) and in good agreement with the PXRD results. The particles display a narrower size distribution and less inter-particle aggregation than HKUST-1, suggesting a more homogeneous nucleation environment under the reflux conditions employed. The absence of collapsed or defect-rich surface regions confirms that the framework retains structural integrity through synthesis and thermal activation, despite the known moisture sensitivity of MOF-5 (Greathouse and Allendorf, 2006). The contrasting crystal habits — octahedral aggregates versus discrete cubic particles — yield different external surface areas, diffusion boundary-layer thicknesses, and intraparticle transport path lengths that directly influence the kinetic behavior discussed in Section 3.7.

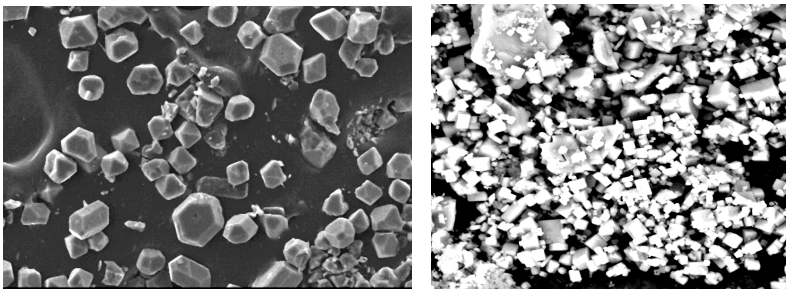

a) b)

Fig. 7. SEM images of (a) HKUST-1, showing well-defined polyhedral crystals with characteristic octahedral morphology (mean equivalent diameter ≈ 26.7 μm), and (b) MOF-5, exhibiting discrete cubic crystals with smooth faces and a uniform particle size distribution.

3.4 Textural Properties and Porosity Analysis

N_2 adsorption–desorption isotherms at 77 K (Figs. 8 and 9) classify both materials as Type I by the IUPAC convention (Sing et al., 1985), confirming a predominantly microporous character. HKUST-1 shows a sharp uptake onset at very low relative pressures ($P/P_0 < 0.01$), indicative of rapid micropore filling driven by strong host–guest interactions; the semilogarithmic inset in Fig. 8 highlights this region. The calculated BET surface area is 1420 $m^2\ g^{-1}$ (Brunauer et al., 1938), with a total pore volume of 0.70 $cm^3\ g^{-1}$, of which 0.62 $cm^3\ g^{-1}$ is micropore volume (Table 1). MOF-5 displays a significantly higher adsorption plateau, consistent with its larger BET surface area (2886 $m^2\ g^{-1}$) and total pore volume (1.15 $cm^3\ g^{-1}$; micropore volume = 1.07 $cm^3\ g^{-1}$; Table 1). DFT pore-size distributions (Figs. 10 and 11) confirm the predominance of narrow micropores in both materials, with well-defined distributions that reflect the ordered pore architectures of each framework (Lowell et al., 2004). A minor mesoporosity contribution (≈ 0.08 $cm^3\ g^{-1}$ in both cases) is attributed to inter-particle voids rather than to structural mesopores. These textural parameters provide the quantitative basis for rationalizing the differential adsorption capacities described in Section 3.6.

Table 1. Textural parameters of HKUST-1 (MOF-199) and MOF-5 obtained from N_2 adsorption–desorption isotherms at 77 K.

Sample	S_{BET} ($m^2\ g^{-1}$)	$S_{Langmuir}$ ($m^2\ g^{-1}$)	V_{total} ($cm^3\ g^{-1}$)	V_{micro} ($cm^3\ g^{-1}$)	V_{meso} ($cm^3\ g^{-1}$)
HKUST-1	1420	1485	0.70	0.62	0.08
MOF-5	2886	2908	1.15	1.07	0.08

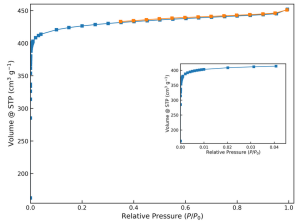

Fig. 8. N_2 adsorption–desorption isotherm of HKUST-1 at 77 K, exhibiting Type I behavior characteristic of microporous materials. Inset: semilogarithmic representation highlighting the low-pressure region associated with micropore filling.

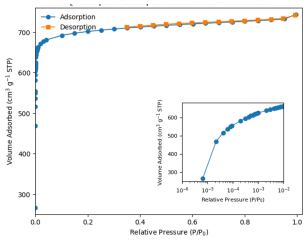

Fig. 9. N_2 adsorption–desorption isotherm of MOF-5 at 77 K. Inset: semilogarithmic representation of the low-pressure region.

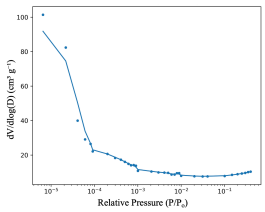

Fig. 10. DFT pore-size distribution of HKUST-1 derived from N_2 adsorption data, confirming predominant narrow micropore character.

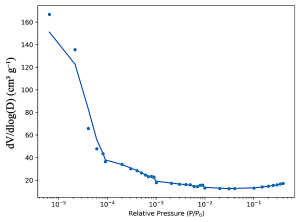

Fig. 11. DFT pore-size distribution of MOF-5 derived from N_2 adsorption data, confirming a narrow, highly ordered micropore structure.

3.5 Hydrolytic Stability of HKUST-1 and MOF-5

Before proceeding with adsorption experiments, the hydrolytic stability of both frameworks was systematically evaluated by immersion in buffered aqueous solutions at pH 3–9. Post-immersion PXRD patterns of HKUST-1 showed progressive broadening and attenuation of characteristic reflections at pH > 5, accompanied by a marked

reduction in BET surface area and the appearance of new FTIR absorptions consistent with copper hydroxide or copper oxide species — clear evidence of partial framework decomposition triggered by water attack on the Cu–carboxylate coordination bonds, consistent with the findings of Kúsgens et al. (2009) and Schoenecker et al. (2012). MOF-5 exhibited even greater sensitivity: near-complete amorphization was observed above pH 5, with essentially complete porosity collapse at neutral and alkaline pH, consistent with the well-known susceptibility of Zn–carboxylate linkages to hydrolysis reported by Greathouse and Allendorf (2006) and Huang et al. (2003). These observations confirm that neither material is suitable for direct application in conventional aqueous treatment systems without structural stabilization (Wang et al., 2015; Canivet et al., 2014), providing unambiguous experimental justification for the non-aqueous experimental design adopted throughout this work. Both materials were confirmed to be fully stable in absolute ethanol throughout all adsorption experiments, as verified by post-adsorption PXRD and FTIR characterization, thereby validating the integrity and interpretability of all reported adsorption parameters.

3.6 Adsorption Equilibrium

The equilibrium adsorption isotherms of diclofenac on HKUST-1 and MOF-5, measured at 298 K in absolute ethanol, are compared in Fig. 12. Both profiles exhibit a Type I shape — a steep initial uptake at low equilibrium concentrations followed by a gradual approach to a well-defined plateau — consistent with micropore-controlled adsorption, in which a finite number of active sites are progressively occupied until saturation (Sing et al., 1985). MOF-5 achieves a substantially higher maximum equilibrium uptake (exceeding 200 mg g^{-1}), whereas HKUST-1 saturates at approximately 120 mg g^{-1} under identical conditions. This approximately twofold difference in capacity closely parallels the ratio of BET surface areas (2886 vs. 1420 m^2 g^{-1}) and the larger total pore volume of MOF-5 (Table 1), both of which provide greater accommodation volume for diclofenac molecules. In contrast, HKUST-1 displays a markedly steeper initial slope, reflecting a substantially higher initial adsorption affinity consistent with the presence of coordinatively unsaturated Cu(II) open metal sites (OMS) within the paddle-wheel SBUs, which engage in specific Lewis acid–base and electrostatic interactions with the carboxylate and chlorine substituents of diclofenac (Chui et al., 1999; Prestipino et al., 2006).

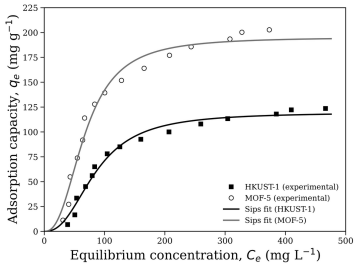

Fig. 12. Comparative adsorption isotherms of diclofenac on HKUST-1 and MOF-5 in absolute ethanol at 298 K. Symbols represent experimental data; solid lines correspond to Sips model fits, which provided the best statistical description for both materials based on R^2, RMSE, and AIC (Table 2).

The experimental data were fitted simultaneously to the Langmuir (Langmuir, 1918), Freundlich (Freundlich, 1906), and Sips (Sips, 1948) isotherm models using nonlinear least-squares regression; parameter estimates and goodness-of-fit statistics are compiled in Table 2. The Sips model — which combines Freundlich-type behavior at low surface coverage with the saturation-limiting behavior of the Langmuir model at high concentrations and introduces a heterogeneity exponent n — provided the best overall statistical description for both materials, as indicated by the highest R^2 values (0.9806 for HKUST-1 and 0.9767 for MOF-5), the lowest RMSE, and the lowest AIC (Table 2). The Sips maximum adsorption capacities are 119.61 mg g^{-1} for HKUST-1 and 195.28 mg g^{-1} for MOF-5. The heterogeneity exponent $n > 1$ for both materials indicates adsorption on energetically heterogeneous surfaces, fully consistent with the multimodal pore architectures and chemical diversity of the framework surfaces (Prasetya and Li, 2021). The Langmuir model overestimates qmax (181.45 and 295.18 mg g^{-1} for HKUST-1 and MOF-5, respectively) and shows poorer statistical performance (Zhuang et al., 2019). The Freundlich model performs least well in the saturation region, as expected for an empirical power-law expression lacking a physically motivated capacity limit (Freundlich, 1906). From a mechanistic perspective, adsorption on MOF-5 is primarily governed by pore filling and non-specific dispersion interactions (London forces) between the aromatic π-system of diclofenac and the BDC-derived aromatic walls of the pore interior (Hasan et al., 2012). HKUST-1 combines these contributions with stronger, more localized interactions at OMS, yielding higher initial adsorption affinity despite its lower overall capacity (Crespí Sánchez et al., 2023). The non-aqueous medium is decisive in this context: in aqueous systems, water molecules would

preferentially occupy OMS through competitive coordination, eliminating the interaction sites responsible for the high affinity of HKUST-1 and simultaneously degrading the framework through progressive hydrolysis (Kúsgens et al., 2009). The non-aqueous strategy thus not only preserves structural integrity but also reveals interaction modes that would be systematically obscured in conventional aqueous evaluations (DeCoste et al., 2012).

Table 2. Isotherm model parameters for diclofenac adsorption onto HKUST-1 and MOF-5 in absolute ethanol at 298 K, obtained from nonlinear regression of Langmuir, Freundlich, and Sips models. qmax: maximum adsorption capacity; K_L, K_F, K_S: model equilibrium constants; n: heterogeneity exponent.

Material	Model	q_{max} (mg g^{-1})	K_L / K_F / K_S	n	R^2	RMSE
HKUST-1	Langmuir	181.45	5.40×10^{-3}	—	0.9189	10.68
HKUST-1	Freundlich	—	5.30	1.890	0.8590	14.08
HKUST-1	Sips	119.61	1.17×10^{-2}	2.458	0.9806	5.23
MOF-5	Langmuir	295.18	6.90×10^{-3}	—	0.9138	18.01
MOF-5	Freundlich	—	10.08	1.909	0.8532	23.50
MOF-5	Sips	195.28	1.48×10^{-2}	2.493	0.9767	9.36

3.7 Adsorption Kinetics and Diffusion Mechanism

The time-resolved adsorption profiles of diclofenac on HKUST-1 and MOF-5 share a common qualitative pattern: rapid initial uptake during the first 60–120 min, driven by abundant external surface sites and a steep concentration gradient, followed by a progressively slower approach to equilibrium as internal diffusional resistance becomes increasingly dominant (Ho and McKay, 1999). A quantitative comparison of the three kinetic models (Table 3) shows that the PFO equation (Lagergren, 1898) provides the best overall statistical fit for both materials — the highest R^2 values (0.8291 for HKUST-1 and 0.8583 for MOF-5) and the lowest RMSE and AIC — while the PFO-predicted equilibrium capacities ($q_{e,cal}$ = 138.96 and 123.11 mg g^{-1}) agree closely with the experimental values (138.50 and 124.70 mg g^{-1}), confirming the physical meaningfulness of the fit. The PSO model (Ho and McKay, 1999) yields overestimated qe values and inferior statistical metrics, indicating that a bimolecular surface reaction is not the primary rate-controlling mechanism. The Elovich model (Elovich and Larionov, 1962) — which assumes an exponentially decreasing adsorption rate consistent with surface energy heterogeneity — provides a reasonable but statistically inferior description (Table 3), in agreement with the energetic heterogeneity already established by the Sips isotherm analysis.

Table 3. Kinetic model parameters for diclofenac adsorption onto HKUST-1 and MOF-5 in absolute ethanol at 298 K, obtained from nonlinear regression of pseudo-first-order (PFO), pseudo-second-order (PSO), and Elovich model

Material	Model	Parameter 1	Parameter 2	$Q_{,exp}$ (mg g^{-1})	$q_{e,cal}$ (mg g^{-1})	R^2	RMSE
HKUST-1	PFO	k_1 = 0.0187 min^{-1}	—	138.50	138.96	0.8291	18.83
HKUST-1	PSO	k_2 = 1.00×10^{-4} g mg^{-1} min^{-1}	—	138.50	165.42	0.8102	19.84
HKUST-1	Elovich	α = 4.63 mg g^{-1} min^{-1}	β = 0.025 g mg^{-1}	138.50	—	0.7787	21.42
MOF-5	PFO	k_1 = 0.0288 min^{-1}	—	124.70	123.11	0.8583	15.43
MOF-5	PSO	k_2 = 2.00×10^{-4} g mg^{-1} min^{-1}	—	124.70	140.10	0.8422	16.28

MOF-5	Elovich	α = 7.23 mg g⁻¹ min⁻¹	β = 0.033 g mg⁻¹	124.70	—	0.8046	18.12

Further insight into the transport mechanism is provided by the Weber–Morris intraparticle diffusion plots (Fig. 13; Weber and Morris, 1963), in which both materials exhibit clear multilinear behavior with three well-defined segments. Zone I corresponds to rapid external film diffusion across the hydrodynamic boundary layer at the solid–solution interface. Zone II represents the rate-limiting intraparticle diffusion step, during which diclofenac molecules migrate progressively into the micropore network against increasing diffusional resistance. Zone III is the near-horizontal plateau region associated with final surface equilibration. The non-zero y-intercepts of the Zone II fitted lines for both materials confirm that intraparticle diffusion is not the sole rate-controlling step and that external mass transfer exerts a measurable co-limiting influence on the overall kinetics (Weber and Morris, 1963; Tan et al., 2008) — a result consistent with the relatively large crystal sizes observed by SEM and the hierarchical transport pathway from bulk solution into the micropore network.

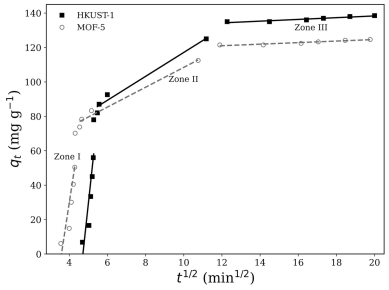

Fig. 13. Weber–Morris intraparticle diffusion plots (qt vs $t^{1/2}$) for diclofenac adsorption on HKUST-1 and MOF-5 in absolute ethanol at 298 K. Three distinct linear regions are identified: Zone I (external mass transfer), Zone II (intraparticle diffusion), and Zone III (equilibrium stage). The non-zero intercepts of the Zone II lines indicate that intraparticle diffusion is not the sole rate-controlling step.

The quantitative Weber–Morris parameters are summarized in Table 4. The Zone II intraparticle diffusion constants (kid) are slightly higher for HKUST-1 (6.95 mg g⁻¹ min⁻¹/²) than for MOF-5 (5.77 mg g⁻¹ min⁻¹/²), suggesting slightly faster solute transport within MOF-5's more open pore network. The substantially larger boundary-layer intercept values (C) for HKUST-1 (47.61 mg g⁻¹ in Zone II) indicate more pronounced external mass-transfer resistance, consistent with its larger mean crystal size and compact octahedral morphology (Hasan et al., 2012). The multistep kinetic behavior is fully consistent with the hierarchical pore structure and contrasting crystal habits established in Section 3.3.

Table 4. Weber–Morris intraparticle diffusion parameters for diclofenac adsorption onto HKUST-1 and MOF-5 in absolute ethanol at 298 K. kid: intraparticle diffusion rate constant (mg g⁻¹ min⁻¹/²); C: boundary-layer intercept (mg g⁻¹).

Material	Region	k_{id} (mg g⁻¹ min⁻¹/²)	C (mg g⁻¹)	R^2	RMSE
HKUST-1	Zone I	102.90	−485.42	0.7563	11.77
HKUST-1	Zone II	6.95	47.61	0.9778	2.50
HKUST-1	Zone III	0.51	128.21	0.9073	0.42
MOF-5	Zone I	72.74	−261.32	0.7493	10.76
MOF-5	Zone II	5.77	50.76	0.9800	2.14
MOF-5	Zone III	0.45	115.61	0.9059	0.38

3.8 Thermodynamic Analysis

The thermodynamic parameters for diclofenac adsorption onto HKUST-1 and MOF-5 were evaluated from equilibrium data collected at 283, 288, 293, and 298 K and are compiled in Table 5. Across the entire temperature range, the standard Gibbs free energy change ΔG° is negative for both materials, confirming that adsorption is thermodynamically spontaneous under all studied conditions (Liu, 2009):

$$\Delta G^o = -RTlnk_c$$

The progressive increase in the magnitude of ΔG° with decreasing temperature — increasingly negative values at lower temperatures — indicates that the process becomes thermodynamically more favorable as temperature decreases, the expected signature of an exothermic system (Foo and Hameed, 2010). This trend is more pronounced for HKUST-1 (ΔG° from −23.9 kJ mol⁻¹ at 298 K to −26.2 kJ mol⁻¹ at 283 K) than for MOF-5 (ΔG° ≈ −21.8 kJ mol⁻¹ throughout), reflecting the stronger enthalpic driving force in the Cu-containing framework. The standard enthalpy change ΔH° is negative for both materials (Table 5): −48.6 kJ mol⁻¹ for HKUST-1 and −21.4 kJ mol⁻¹ for MOF-5, as derived from the van't Hoff relation:

$$lnK_c = \left(\frac{\Delta H^o}{RT}\right) + \left(\frac{\Delta S^o}{R}\right)$$

These values fall within the generally accepted energetic boundaries that distinguish chemisorption (> 40 kJ mol⁻¹) from physisorption (< 40 kJ mol⁻¹), providing thermodynamic corroboration for the interaction mechanisms inferred from equilibrium and structural analyses (Liu, 2009; Foo and Hameed, 2010). The large negative ΔH° of HKUST-1 is consistent with strong, localized interactions between diclofenac and open Cu(II) coordination sites, whereas the smaller magnitude for MOF-5 reflects weaker, non-specific dispersion interactions in a more purely physisorptive regime (Zhuang et al., 2019). The entropy change ΔS° is negative for HKUST-1 (−75.2 J mol⁻¹ K⁻¹), indicating a net decrease in translational and rotational degrees of freedom at the solid–solution interface upon adsorption — a consequence of the highly ordered, site-specific binding geometry imposed by coordinative Cu–diclofenac interactions (Tan et al., 2008). The slightly positive ΔS° for MOF-5 (+1.3 J mol⁻¹ K⁻¹) suggests a marginal increase in total entropy, plausibly from partial displacement and release of ethanol molecules as diclofenac enters the pore space (Hasan et al., 2012). The highly linear van't Hoff fits (R^2 = 0.995 and 0.991 for HKUST-1 and MOF-5, respectively) validate the thermodynamic consistency of the results over the studied temperature range (Liu, 2009).

Table 5. Thermodynamic parameters for diclofenac adsorption onto HKUST-1 and MOF-5 derived from van't Hoff analysis. ΔH° and ΔS° were obtained from the slope and intercept of the linear van't Hoff plot (ln Kc vs. 1/T).

Material	T (K)	ΔG° (kJ mol⁻¹)	ΔH° (kJ mol⁻¹)	ΔS° (J mol⁻¹ K⁻¹)	R^2	Adsorption character
HKUST-1	283	−26.2	−48.6	−75.2	0.995	Chemisorption; spontaneous, exothermic, ordered
	288	−25.5				
	293	−24.7				
	298	−23.9				
MOF-5	283	−21.8	−21.4	+1.3	0.991	Physisorption; spontaneous, weakly exothermic
	288	−21.8				
	293	−21.8				
	298	−21.8				

Viewed collectively, the thermodynamic results reinforce the mechanistic picture developed from the equilibrium and kinetic analyses. HKUST-1 binds diclofenac with greater energetic favorability and site specificity, driven primarily

by strong enthalpic interactions at OMS, whereas MOF-5 accommodates larger total quantities through weaker but more numerous pore-filling interactions (Foo and Hameed, 2010). This complementary behavior highlights a fundamental principle for adsorbent design: neither surface area nor framework chemistry alone determines adsorption performance; both must be considered jointly (Furukawa et al., 2013; Zhao et al., 2018). The dual-parameter design logic — quantified here through the non-aqueous strategy — guides the engineering of next-generation, water-stable MOF adsorbents that combine high pore-filling capacity with targeted chemical affinity at metal coordination sites, a design objective directly relevant to pharmaceutical micropollutant removal in sustainable wastewater treatment (Ali, 2012; Barbosa et al., 2016).

4. Conclusions

This study demonstrates that a rigorously controlled non-aqueous experimental strategy yields reliable, interpretable adsorption data for hydrolytically sensitive MOFs, revealing intrinsic structure–property relationships that aqueous evaluations systematically obscure. The principal findings are as follows.

Reflux-based synthesis yields HKUST-1 and MOF-5 with phase purity, crystallinity, and textural properties (S_{BET} = 1420 and 2886 $m^2\ g^{-1}$, respectively) comparable to those from conventional solvothermal routes, validating this operationally accessible and energy-efficient approach for producing structurally robust frameworks at scale. The similarity of results to established autoclave-based protocols is particularly relevant for groups working in resource-limited environments.

Systematic hydrolytic stability testing across pH 3–9 established that neither framework is structurally suitable for direct aqueous application without chemical stabilization, providing unambiguous experimental justification for the non-aqueous design and highlighting a methodological gap in the broader MOF adsorption literature, where analogous stability verification is rarely reported. Post-adsorption characterization confirmed that both materials retained their crystalline integrity throughout all experiments conducted in absolute ethanol.

Diclofenac adsorption in absolute ethanol is best described by the Sips isotherm ($R^2 > 0.97$ for both materials), confirming energetically heterogeneous surface interactions. MOF-5 achieves higher capacity (195.28 mg g^{-1}) due to its larger pore volume and surface area, whereas HKUST-1 displays superior adsorption affinity attributable to specific interactions at coordinatively unsaturated Cu(II) open metal sites.

Kinetic profiles exhibit pseudo-first-order behavior, and Weber–Morris multilinear analysis confirms a multistep transport mechanism in which external boundary-layer diffusion and intraparticle diffusion act as co-limiting steps. The more pronounced boundary-layer resistance of HKUST-1 is consistent with its larger crystal size and compact octahedral morphology.

Thermodynamic analysis confirms that adsorption is spontaneous and exothermic for both materials. The large negative $\Delta H°$ of HKUST-1 (−48.6 kJ mol^{-1}) is consistent with chemisorption, whereas the smaller value for MOF-5 (−21.4 kJ mol^{-1}) indicates a physisorption regime — a thermodynamic distinction consistent with all structural and kinetic evidence.

Beyond these material-specific findings, the non-aqueous methodology established here provides a reproducible, transparent platform for generating reliable structure–property correlations in MOF-based adsorption science. This framework offers a principled basis for the rational design of water-stable, structurally reinforced MOF variants that combine the high capacity of open-pore architectures with the targeted chemical affinity of metal coordination sites — a design objective directly relevant to the growing challenge of removing pharmaceutical micropollutants within sustainable wastewater management and cleaner waste systems.

Acknowledgements

The authors acknowledge the interinstitutional framework agreement between Universidad de los Andes and the Universidad Nacional de Colombia (Bogotá Campus) and the financial support from the Faculty of Sciences at Universidad de los Andes through project INV-2025-213-3457. The authors also thank the technical staff at the characterization facilities of both institutions for their assistance with PXRD, SEM, and N_2 adsorption measurements.

Declaration of Competing Interest

The authors declare that they have no known competing financial interests or personal relationships that could have appeared to influence the work reported in this paper.

References

Ali, I., 2012. New generation adsorbents for water treatment. *Chem. Rev.* 112, 5073–5091. https://doi.org/10.1021/cr300133d

Barbosa, M.O., Moreira, N.F.F., Ribeiro, A.R., Pereira, M.F.R., Silva, A.M.T., 2016. Occurrence and removal of organic micropollutants: an overview of the watch list of EU Decision 2015/495. *Water Res.* 94, 257–279. https://doi.org/10.1016/j.watres.2016.02.047

Bordiga, S., Lamberti, C., Ricchiardi, G., Regli, L., Bonino, F., Damin, A., Lillerud, K.-P., Bjorgen, M., Zecchina, A., 2004. Electronic and vibrational properties of a MOF-5 metal–organic framework: ZnO quantum dot behaviour. *Chem. Commun.* 2300–2301. https://doi.org/10.1039/B407246D

Brunauer, S., Emmett, P.H., Teller, E., 1938. Adsorption of gases in multimolecular layers. *J. Am. Chem. Soc.* 60, 309–319. https://doi.org/10.1021/ja01269a023

Canivet, J., Fateeva, A., Guo, Y., Coasne, B., Farrusseng, D., 2014. Water adsorption in MOFs: fundamentals and applications. *Chem. Soc. Rev.* 43, 5594–5617. https://doi.org/10.1039/C4CS00078A

Chui, S.S.-Y., Lo, S.M.-F., Charmant, J.P.H., Orpen, A.G., Williams, I.D., 1999. A chemically functionalizable nanoporous material $[Cu_3(TMA)_2(H_2O)_3]_n$. *Science* 283, 1148–1150. https://doi.org/10.1126/science.283.5405.1148

Crespí Sánchez, N., Turnes Palomino, G., Palomino Cabello, C., 2023. Sulfonic-functionalized MIL-100(Fe) metal–organic framework for diclofenac removal from aqueous solutions. *Microporous Mesoporous Mater.* 348, 112398. https://doi.org/10.1016/j.micromeso.2022.112398

DeCoste, J.B., Peterson, G.W., Schindler, B.J., Killops, K.L., Browe, M.A., Mahle, J.J., 2013. The effect of water adsorption on the structure of the carboxylate containing metal–organic frameworks Cu-BTC, Mg-MOF-74, and UiO-66. *J. Mater. Chem. A* 1, 11922–11932. https://doi.org/10.1039/C3TA12497E

Elovich, S.Y., Larionov, O.G., 1962. Theory of adsorption from solutions of non-electrolytes on solid (I): equation adsorption from solutions and the analysis of its simplest form. *Izv. Akad. Nauk SSSR, Otd. Khim. Nauk* 2, 209–216.

European Commission, 2013. Directive 2013/39/EU amending Directives 2000/60/EC and 2008/105/EC as regards priority substances in the field of water policy. *Off. J. Eur. Union* L 226, 1–17.

Foo, K.Y., Hameed, B.H., 2010. Insights into the modeling of adsorption isotherm systems. *Chem. Eng. J.* 156, 2–10. https://doi.org/10.1016/j.cej.2009.09.013

Freundlich, H., 1906. Über die adsorption in Lösungen. *Z. Phys. Chem.* 57, 385–470. https://doi.org/10.1515/zpch-1907-5723

Furukawa, H., Cordova, K.E., O'Keeffe, M., Yaghi, O.M., 2013. The chemistry and applications of metal-organic frameworks. *Science* 341, 1230444. https://doi.org/10.1126/science.1230444

Greathouse, J.A., Allendorf, M.D., 2006. The interaction of water with MOF-5 simulated by molecular dynamics. *J. Am. Chem. Soc.* 128, 10678–10679. https://doi.org/10.1021/ja063506b

Hasan, Z., Jeon, J., Jhung, S.H., 2012. Adsorptive removal of naproxen and clofibric acid from water using metal-organic frameworks. *J. Hazard. Mater.* 209–210, 151–157. https://doi.org/10.1016/j.jhazmat.2012.01.005

Hernando, M.D., Mezcua, M., Fernández-Alba, A.R., Barceló, D., 2006. Environmental risk assessment of pharmaceutical residues in wastewater effluents, surface waters and sediments. *Talanta* 69, 334–342. https://doi.org/10.1016/j.talanta.2005.09.037

Ho, Y.S., McKay, G., 1999. Pseudo-second order model for sorption processes. *Process Biochem.* 34, 451–465. https://doi.org/10.1016/S0032-9592(98)00112-5

Huang, L., Wang, H., Chen, J., Wang, Z., Sun, J., Zhao, D., Yan, Y., 2003. Synthesis, morphology control, and properties of porous metal–organic coordination polymers. *Microporous Mesoporous Mater.* 58, 105–114. https://doi.org/10.1016/S1387-1811(02)00609-1

Kümmerer, K., 2009. Antibiotics in the aquatic environment — a review. Part I. *Chemosphere* 75, 417–434. https://doi.org/10.1016/j.chemosphere.2008.11.086

Kúsgens, P., Rose, M., Senkovska, I., Fröde, H., Henschel, A., Siegle, S., Kaskel, S., 2009. Characterization of metal–organic frameworks by water adsorption. *Microporous Mesoporous Mater.* 120, 325–330. https://doi.org/10.1016/j.micromeso.2008.11.020

Lagergren, S., 1898. Zur Theorie der sogenannten Adsorption gelöster Stoffe. *K. Sven. Vetenskapsakademiens Handl.* 24, 1–39.

Langmuir, I., 1918. The adsorption of gases on plane surfaces of glass, mica and platinum. *J. Am. Chem. Soc.* 40, 1361–1403. https://doi.org/10.1021/ja02242a004

Li, H., Eddaoudi, M., O'Keeffe, M., Yaghi, O.M., 1999. Design and synthesis of an exceptionally stable and highly porous metal-organic framework. *Nature* 402, 276–279. https://doi.org/10.1038/46248

Liu, Y., 2009. Is the free energy change of adsorption correctly calculated? *J. Chem. Eng. Data* 54, 1981–1985. https://doi.org/10.1021/je800661q

Lowell, S., Shields, J.E., Thomas, M.A., Thommes, M., 2004. *Characterization of Porous Solids and Powders: Surface Area, Pore Size and Density.* Springer, Dordrecht. https://doi.org/10.1007/978-1-4020-2303-3

Prasetya, N., Li, K., 2021. MOF-808 and its hollow fiber adsorbents for efficient diclofenac removal from water. *Chem. Eng. J.* 417, 129216. https://doi.org/10.1016/j.cej.2021.129216

Prestipino, C., Regli, L., Vitillo, J.G., Bonino, F., Damin, A., Lamberti, C., Zecchina, A., Solari, P.L., Kongshaug, K.O., Bordiga, S., 2006. Local structure of framework Cu(II) in HKUST-1 metallorganic framework: spectroscopic characterization upon activation and interaction with adsorbates. *Chem. Mater.* 18, 1337–1346. https://doi.org/10.1021/cm052191g

Schoenecker, P.M., Carson, C.G., Jasuja, H., Flemming, C.J.J., Walton, K.S., 2012. Effect of water adsorption on retention of structure and surface area of metal–organic frameworks. *Ind. Eng. Chem. Res.* 51, 6513–6519. https://doi.org/10.1021/ie202325p

Sing, K.S.W., Everett, D.H., Haul, R.A.W., Moscou, L., Pierotti, R.A., Rouquérol, J., Siemieniewska, T., 1985. Reporting physisorption data for gas/solid systems with special reference to the determination of surface area and porosity. *Pure Appl. Chem.* 57, 603–619. https://doi.org/10.1351/pac198557040603

Sips, R., 1948. On the structure of a catalyst surface. *J. Chem. Phys.* 16, 490–495. https://doi.org/10.1063/1.1746922

Tan, I.A.W., Ahmad, A.L., Hameed, B.H., 2008. Adsorption of basic dye using activated carbon prepared from oil palm shell: batch and fixed bed studies. *Desalination* 225, 13–28. https://doi.org/10.1016/j.desal.2007.07.005

Ternes, T.A., 1998. Occurrence of drugs in German sewage treatment plants and rivers. *Water Res.* 32, 3245–3260. https://doi.org/10.1016/S0043-1354(98)00099-2

Verlicchi, P., Al Aukidy, M., Zambello, E., 2012. Occurrence of pharmaceutical compounds in urban wastewater: removal, mass load, and environmental risk after a secondary treatment. *Sci. Total Environ.* 429, 123–155. https://doi.org/10.1016/j.scitotenv.2012.04.028

Wang, C., Liu, X., Keser Demir, N., Chen, J.P., Li, K., 2015. Applications of water stable metal–organic frameworks. *Chem. Soc. Rev.* 45, 5107–5134. https://doi.org/10.1039/C5CS00757G

Weber, W.J., Morris, J.C., 1963. Kinetics of adsorption on carbon from solution. *J. Sanit. Eng. Div., Am. Soc. Civ. Eng.* 89, 31–60. https://doi.org/10.1061/JSEDAI.0000430

Yaghi, O.M., O'Keeffe, M., Ockwig, N.W., Chae, H.K., Eddaoudi, M., Kim, J., 2003. Reticular synthesis and the design of new materials. *Nature* 423, 705–714. https://doi.org/10.1038/nature01650

Zhao, X., Wang, Y., Li, D.S., Bu, X., Feng, P., 2018. Metal–organic frameworks for separation. *Adv. Mater.* 30, 1705189. https://doi.org/10.1002/adma.201705189

Zhuang, S., Rong, C., Wang, J., Chen, W., Li, X., 2019. Adsorption of diclofenac from aqueous solution using UiO-66-type metal–organic frameworks. *Chem. Eng. J.* 359, 354–364. https://doi.org/10.1016/j.cej.2018.11.150